Highly multimodal structure of high topological charge extreme ultraviolet vortex beams

F. Sanson, A. Pandey, I. Papagiannouli, F. Harms, G. Dovillaire, E. Baynard, J. Demailly, O. Guilbaud, B. Lucas, O. Neveu, et al.

Highly multimodal structure of high topological charge Extreme Ultraviolet vortex beams

F. Sanson[1,2], A. K. Pandey[1], I. Papagiannouli[1], F. Harms[3], G. Dovillaire[3], E. Baynard[4], J. Demailly[1], O. Guilbaud[1], B. Lucas[1], O. Neveu[1], M. Pittman[4], D. Ros[1], M. Richardson[5], E. Johnson[6], W. Li[6], Ph. Balcou[7], and S. Kazamias[1]

[1] Université Paris-Saclay, CNRS, Laboratoire de physique des gaz et des plasmas, 91405, Orsay, France.
[2] Amplitude Laser Group, Scientific Business Unit - Lisses Operations, 2/4 rue du Bois Chaland, 91090 Lisses, France
[3] Imagine Optic, 18, rue Charles de Gaulle, 91400 ORSAY, France
[4] Université Paris-Saclay, CNRS, LASERIX, Centre Laser Université Paris Sud, 91405 Orsay, France
[5] University of Central Florida, 4304 Scorpius Street, Orlando, FL 32816-2700, USA
[6] Clemson University, Dept of Electr. & Computer Engineering, Clemson, South Carolina, USA
[7] Université de Bordeaux, CNRS, CEA; Centre Lasers Intenses et Applications (CELIA), UMR 5107, 33405 Talence, France
* Corresponding author: fabrice.sanson@u-psud.fr

Compiled September 1, 2020

Optical beams carrying Orbital Angular Momentum (OAM) are a very active field of research for their prospective applications, especially at short wavelengths. We consider here such beams produced through high-harmonic generation (HHG) in a rare gas and analyze the characterization of their high charge vortex structure by an EUV (Extreme UltraViolet) Hartmann wavefront sensor. We show that such HHG beams are generally composed of a set of numerous vortex modes. The sensitivity of the intensity and phase of the HHG beam to the infrared (IR) laser aberrations is investigated using a deformable mirror.

http://dx.doi.org/10.1364/ao.XX.XXXXXX

Recent works on structured exotic coherent light sources for a wide range of applications have proved the capability of several processes to produce beams carrying orbital angular momentum (OAM) for a large set of wavelengths: from IR (infrared) to EUV (Extreme UltraViolet). Experimental demonstrations were done with visible and IR light by using Metasurfaces [1], Hermite Gaussian conversion with cylindrical lenses converters [2, 3], Q-plates [4], Spatial Light Modulator [5, 6], digital micromirror device [7], spiral phaseplates [8–10], axicon or combinations of these techniques [11, 12].

Some of these techniques were efficiently applied to femtosecond infrared pulses to produce vortex beams in the EUV domain via High order harmonic generation (HHG) in rare gases [13, 14] or on surfaces [15, 16]. They are considered as first approximations of pure Laguerre-Gauss modes $\mathfrak{LG}_{l,p}$ with l and p being the azimuthal and radial quantum numbers. Experimental measurements of the orbital angular momentum l_q for the q^{th} harmonic order of a laser driving field with $l_{IR} = 1$ inferred $l_q \approx q$ from indirect methods, thus confirming the theoretical predictions by [17] concerning the stability of OAM with regards to the propagation effects [18]. However, the still crude nature of the experimental methods used so far on high order orbital beams are unable to ascertain whether the $l_q = q$ expectation is exactly satisfied; studies on low order orbital beams have hinted at an increased complexity of real vortex beams [19, 20]. Based on a direct method, we present here a full characterization of the OAM structure for the 25^{th} harmonic of an infrared driving field with $l_{IR} = 1$ and unravel for the first time its full complexity at high orders.

The characterization of a high order vortex structure is indeed a non-trivial task especially in the EUV domain: in pioneering studies, an interferometric method was presented by [21] but limited to low l orders; another method was proposed in [22] based on the comparison between the experimental intensity profile and the known radial profiles of pure LG modes. The ratio of the ring inner radius by the outer one yields a shape-derived value for l. Unfortunately, around $l = 25$ this spatial parameter cannot be ascertained with an accuracy better than 5 l orders.

For a refined analysis, our experimental characterization was based on a key objective and device : a complete characterization of the EUV beam by means of an EUV Hartmann sensor (or HASO). Use of such an EUV HASO was first proposed in [23] and extended by us to high orders, until 25 [24]. The EUV HASO features a $72 * 72$ matrix of sampling points in the EUV, yielding at each point the beam intensity and the wavevector direction with an angular accuracy of 0.1 μrad, resulting in a wavefront absolute resolution of $\lambda/50$ at $30nm$.

The main experimental setup is identical to that of our previous letter (Figure 1 of [24]). The driving laser field is a titanium-sapphire operating at $815nm$ wavelength, $80fs$ pulse duration. A $l = 1$ vortex phase plate is inserted in the beam, followed after $1m$ by an $11mm$ iris. The laser energy after it is $3.6mJ$. A $0.9m$ focal length lens, located $0.2m$ after the iris, focuses the beam onto a $10mm$ long gas cell filled with a pressure of $23mbar$ of argon, placed at the focus, to generate high harmonics. The laser

and the harmonics then co-propagate up to a thin aluminum filter, opaque to the IR while transmitting most of the EUV without wavefront distortion. The 25th order harmonic is sent to the EUV Hartmann sensor by a multi-layer mirror, acting as a spectral filter centered at 32.6nm, with a 5nm bandwidth. The distance between the cell and the EUV HASO is $1.96 \pm 4cm$.

Fig.1 shows one of the best EUV beam measured on the Hartmann sensor, for which we inferred the phase using the Southwell [25] algorithm implemented in the proprietary software. The global phase variation (peak to valley) along the ring is around 25λ. In different experimental runs corresponding to slightly different conditions, we have measured global phase changes over the ring lower or equal to 25λ.

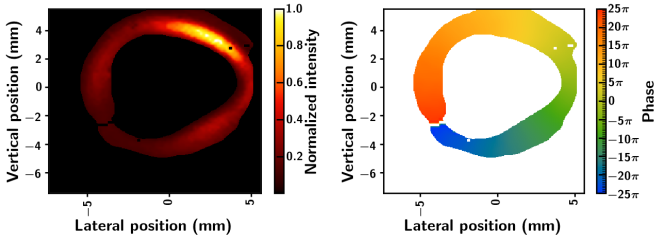

Fig. 1. Reconstructed intensity (left) and phase (right) for the 25th harmonic optical vortex.

The quality of the data from the Hartmann sensor, with a complete 2D mapping of the complex field $E(r,\theta)$, allows us to proceed digitally to a full numerical analysis of the modal content of the beam, both in terms of angular and radial modes, with the following procedure:

All data are first transformed from 4 times oversampled cartesian (x,y) to polar coordinates (r,θ) in order to easily unwrap the azimuthal phase and set the beginning of phase calculation $(\theta = 0)$. The centre of the beam $(r = 0)$ is taken as the point minimizing the sum of distances to all data points, defined as those whose detected intensity is above a noise threshold. Figure 2 shows the unwrapped phase profile corresponding to the beam in fig.1 obtained when substracting a reference phase variation corresponding to an azimuthal order $l_q = 26$, which is the integer that minimizes the phase residual. The right part shows in blue the phase residual after removing $l\theta$ for different l: this indicates that the minimum residual is not zero and even almost constant for l between 24 and 27. This proves that the experimental phase profile can not correspond to a single vortex mode but is actually composed of several modes.

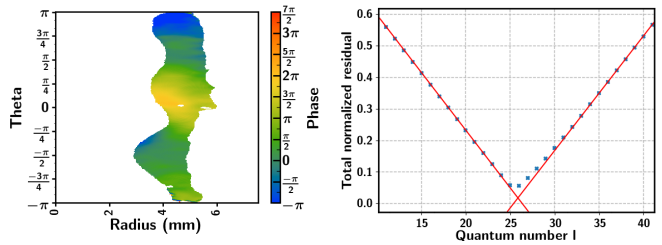

Fig. 2. Phase residual after removing 26θ (left). 2D integral of the absolute phase residual after removing $l\theta$ to the datas, normalized by the value obtained for l= 1 (right). Red fits are crossing at 25.85

We then perform an azimuthal Fourier transform, on the sensor data as in [20]:

$$c_l(r) = \frac{1}{2\pi}\int_0^{2\pi} E(r,\theta)e^{il\theta}d\theta \quad \textbf{(1)}$$

The normalized weight of each azimuthal mode l is given by the radial integration:

$$P(l) = \frac{\int_0^\infty |c_l|^2 rdr}{\sum_l \int_0^\infty |c_l|^2 rdr} \quad \textbf{(2)}$$

Each azimuthal mode l corresponds to a set of radial modes (l,p). The complete 2D mode description is obtained via the Laguerre-Gaussian ($\mathfrak{LG}$) projection:

$$P_{l,p} = |\int_0^{2\pi}\int_0^\infty \mathbf{E}(r,\theta)^* * \mathfrak{LG}_{l,p} rdrd\theta|^2. \quad \textbf{(3)}$$

The number of (l,p) modes for which $P_{l,p}$ can be calculated is theoretically infinite but practically only a finite set of modes corresponds to non negligible values: this constitutes a complete description of the experimental vortex.

Once the center is fixed, the Fourier azimuthal decomposition is unique. However, as outlined in [26], the radial decomposition is not unique, as it depends on the waist $w(z)$ chosen for the description of the $\mathfrak{LG}$ base. This choice has an impact on the number of $\mathfrak{LG}$ modes necessary to describe a beam. We use the fact that the radius r_{max} of maximum intensity for the harmonic ring coincides at the source with the one of the infrared vortex. The waist value corresponding to r_{max} for a given l_q is therefore $w_{l_q} = r_{max}\sqrt{\frac{2}{l_q}}$.

For the $\mathfrak{LG}$ base definition, we calculate the waist $w_{l_q} = 16.7\mu m$ from r_{max} with l_q taken as the closest integer to the average l in the azimuthal Fourier transform: $l_q = 24$. The $\mathfrak{LG}$ base is thus constructed with a constant waist $w_{l_q=24}$ and a l range between 1 and 51 symetric around 25, with 0 order include in the range. An alternative approach, with waist values scaling as $1/\sqrt{l}$, turns out to yield poorer decompositions, meaning an increased number of p components necessary to describe the experimental profiles.

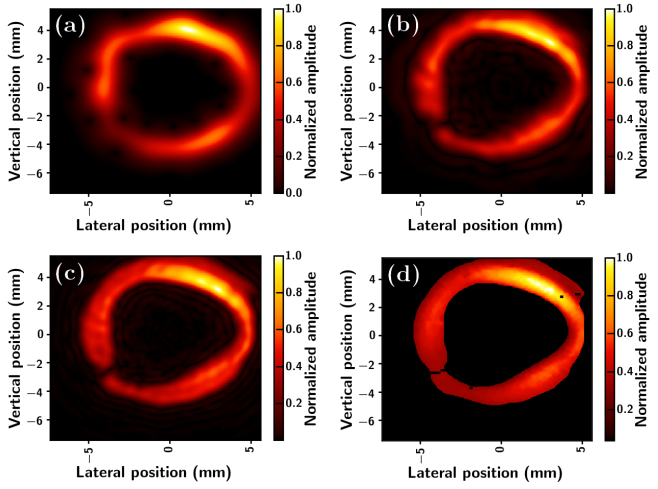

Fig. 3. (a) to (c) : Evolution of reconstructed amplitudes as an increasing number of p orders are summed. (a) $p = 0$ only; (b) p from 0 to 4; (c) p from 0 to 10. (d) : experimental result. l orders from 1 to 51 are included in the reconstructions.

Figure 3 shows that a correct modal analysis of the reference experimental beam from figure 1, requires the summation of a minimum of 5 p values ($p = 0, 1, 2, 3, 4$). A single value of p is obviously not appropriate to describe a HHG vortex beam; this is related to the highly non-linear and non-perturbative nature of the HHG process [27].

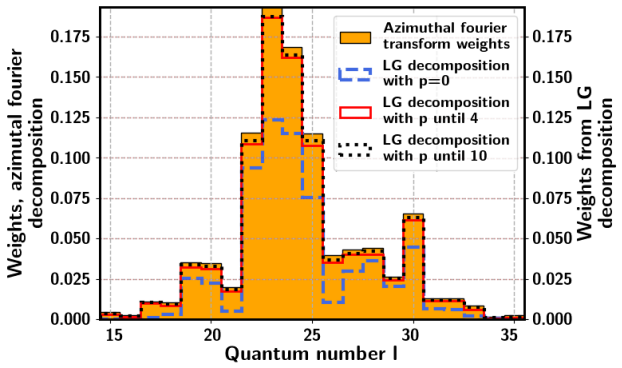

Fig. 4. Comparison between $\mathfrak{LG}$ decomposition for an increasing number of radial modes and azimuthal Fourier transform.

Figure 4 presents a quantitative comparison of the results obtained for the beam of Figure 3 as a function of l with both methods: azimuthal Fourier transform (orange histograms, intrinsically independent of p and waist choice), in blue the $\mathfrak{LG}$ decomposition for $p = 0$ only, in red the sum for p from 0 to 4, in black from 0 to 10. The $\mathfrak{LG}$ sum with $p = 0$ to 10 (and even only with $p = 0$ to 4) is really accurate unlike the one with $p = 0$ only. Note also that choosing smaller or larger values of the waist w_{l_q} results in slower and asymetric convergence with p between the low-l and high-l sides of fig. 4 ; any significant shift in the analysis central point results in a drop in the $p = 0$ component weight and slower convergence. This shows the relevance of

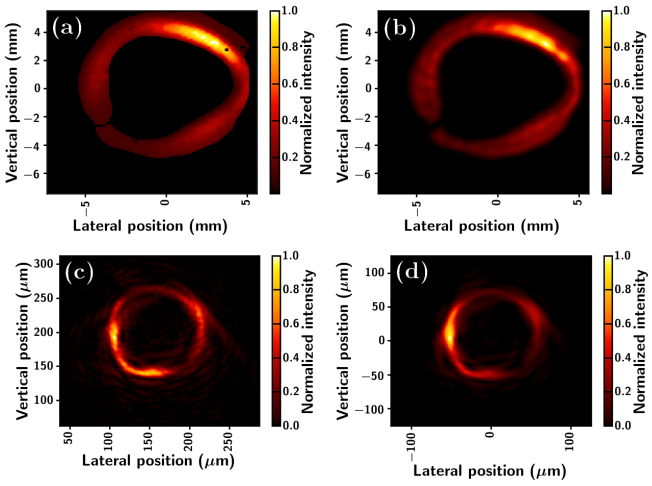

Fig. 5. Comparison between intensity profiles from experimental data ((a) and (c)) and from $\mathfrak{LG}$ decomposition ((b) and (d)) , either at the detection plane ((a) and (b)) or retro-propagated numerically to the source plane, (c) by a full Point Spread Function algorithm, and (d) by a $\mathfrak{LG}$ approach.

our center and waist definitions, and that an EUV Hartmann sensor with appropriate data post-processing is a powerful tool to recover complex beam information, as is illustrated in figure 5, comparing experimental and $\mathfrak{LG}$-reduced data at sensor plane (a and b), and back-propagated profiles at the source plane computed with an extensive PSF (Point Spread Function) algorithm (c) to that obtained via a $\mathfrak{LG}$ reconstruction (d).

Discussions on l distributions such as shown in Fig. 6 often require the intuitive notion of central l, for which we may propose 4 definitions. Two are based on the azimuthal analysis of the complex field: l_{MAX} as the maximum for the azimuthal distribution (23 in fig. 6), and the average l (here 24.3) with its corresponding standard deviation Δl (4.4). They can be compared to estimates from the pure phase data, with the l value giving the lowest phase residual as in fig. 2 (here. 25.8), or the best fit to the radially integrated θ-dependent phase (here 25.5).

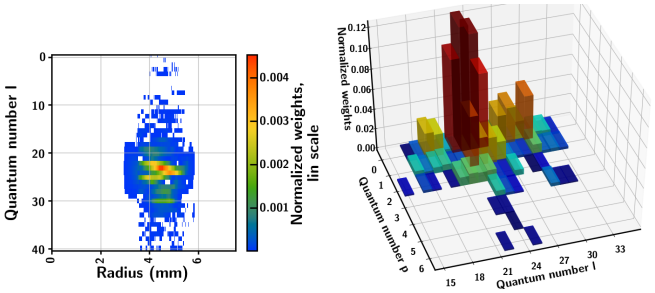

Fig. 6. $\mathfrak{LG}$ decomposition on l and p (right) and azimuthal Fourier transform on l and radius (left)

Both azimuthal Fourier analysis and $\mathfrak{LG}$ decomposition also allow to perform a 2D spatial analysis of the experimental vortex. The azimuthal Fourier distribution, displayed in 6(a), shows that the width of the l distribution may vary radially; and a 3D-plot of the $\mathfrak{LG}$ decomposition (Fig. 6(b)) suggests that the number of significant radial modes p increases around the central l value. This confirms the superiority of these methods over simpler ones to analyse the multimodal structure of the HHG beam.

The role of residual laser aberrations on the modal structure of HHG vortex beams has been studied with a deformable mirror coupled to a wavefront sensor, inducing a controlled level of astigmatism on the pump beam. The initial setting corresponds to a static correction applied after an optimization loop on the IR laser focus. Fig. 7 shows how the central l, defined by the four methods we introduced, is affected by astigmatism. Disregarding the lower l values obtained in this run, which may be due either to slightly different experimental conditions or to a possible systematic calibration offset on the EUV HASO in this campaign, fig. 7 shows that even a small level of astigmatism changes very significantly the central l value: up to 10 l-orders for an astigmatism level of $\lambda/40$. The focused laser profiles are shown in central (optimal beam) and top right insets (maximally aberrated beam).

Whatever the l definition, the global behavior is the same, and whereas no significant widening of Δl with increasing astigmatism is observed, the less aberrant IR beam provides the l value closest to the theoretical prediction ($ql_{IR} = 25$). For IR astigmatism larger than $30nm(\lambda/30)$ the simple phase-only methods are unable to properly describe the beam. In the presence of IR astigmatism and/or with some residual zero order gaussian mode ($l = 0$) coming from the non ideal phase plate conversion [10] the IR photons may carry different individual values of l. From the quantum approach of phase matching [28], the l value for an harmonic photon is the sum of those of all the absorbed IR pho-

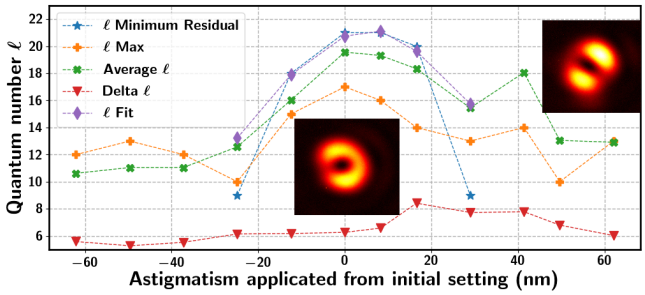

Fig. 7. Blue star : minimum phase residual l; purple diamond : linear regression l from θ-dependent phase; orange and green crosses: l_{Max} and average l from azimuthal Fourier transform; red triangle : standard deviation Δl. Abcissa : RMS added astigmatism on the full beam.

tons (25 for the 25^{th} harmonic order) and may differ from $l_q = q$. In terms of $\mathfrak{LG}$ modes, the astigmatism can be described as the creation of l sidebands, leading to a non pure OAM driving field that strongly influences the HHG modal decomposition.

As a conclusion, we demonstrated that even for harmonic vortex obtained via adaptative optic optimization of the IR pump beam, the modal decomposition is quite large in terms of OAM (azimuthal l and radial p values). This appears unavoidable considering the process used to generate the infrared vortex source [8–10]. Furthermore, the non linear harmonic generation process in the presence of residual astigmatism can be seen to induce additional l bands to the initial IR spectrum, whom effect is described in [29]. We showed that our experimental approach using EUV Hartmann wavefront sensor is able to describe efficiently the highly multimodal vortex structure, and that previous analyses based on monomode hypothesis were first order approximations representing only few percents of the total beam energy for experimental HHG beams. We presented different possible definitions of the l value and consider that the average l from the azimuthal Fourier transform is the most significant since it takes into account both the phase and intensity 2D dependence. This is the macroscopic expression of the superposition of a wide spectrum of integer l values.

The exact mode distribution may be sensitive to instrumentation and post-processing issues such as waist or centre determination, but always displays a consistent span $\pm\Delta l$ of angular momenta, showing the intrinsically multimodal nature of the HHG vortex beam.

Finally, our analysis method gives access to l radial dependency that will allow to study the effects of the HHG atomic process and phase matching on the multimodal structure of the beam, especially in the cases when several rings can clearly be distinguished on the images. Conversely, the use of a deformable mirror could be a way to produce the shape of infrared driving field that would minimize the EUV mode spreading from high order harmonic generation.

Fundings U.S. Army Research Office; LIDEX OPT2X, PULSEX, Université Paris-Saclay; Région Ile de France; Amplitude Technologies Company [Convention Industrielle de Formation par la Recherche (CIFRE) contract].

Acknowledgments The vortex optic was developed with the help of the U.S. Army Research Office. Support was provided by the Idex Paris-Saclay (Lidex Opt2X) and ERM projects and Région Ile-de-France (projects Pulse-X and CPER-POLA) for the wavefront devices. The authors thank the CEMOX installation at IOGS Palaiseau for the multilayer optics and Amplitude Laser Group pour PhD funding.

Disclosures FS : Amplitude Laser Group (F,E); FH, GD : Imagine Optic (E); MR : US Army Research Office (F)

REFERENCES

1. L. Huang, X. Song, B. Reineke, T. Li, X. Li, J. Liu, S. Zhang, Y. Wang, and T. Zentgraf, Acs Photonics **4**, 338 (2017).
2. L. Allen, M. W. Beijersbergen, R. Spreeuw, and J. Woerdman, Phys. Rev. A **45**, 8185 (1992).
3. R. Uren, S. Beecher, C. R. Smith, and W. A. Clarkson, IEEE J. Quantum Electron. (2019).
4. A. Rubano, F. Cardano, B. Piccirillo, and L. Marrucci, J. Opt. Soc. Am. B **36**, D70 (2019).
5. T. W. Clark, R. F. Offer, S. Franke-Arnold, A. S. Arnold, and N. Radwell, Opt. Express **24**, 6249 (2016).
6. T. Ando, Y. Ohtake, N. Matsumoto, T. Inoue, and N. Fukuchi, Opt. Lett. **34**, 34 (2009).
7. Y.-X. Ren, R.-D. Lu, and L. Gong, Ann. Phys. **527**, 447 (2015).
8. M. Beijersbergen, Opt. Comm. **112**, 321 (1994).
9. K. Sueda, G. Miyaji, N. Miyanaga, and M. Nakatsuka, Opt. Express **12**, 3548 (2004).
10. A. Longman and R. Fedosejevs, Opt. Express **25**, 17382 (2017).
11. G. Machavariani, N. Davidson, E. Hasman, S. Blit, A. Ishaaya, and A. Friesem, Opt. Comm. **209**, 265 (2002).
12. Y. Shen, X. Wang, Z. Xie, and X. Yuan, Light. Sci. & Appl. **8**, 90 (2019).
13. G. Gariepy, J. Leach, K. T. Kim, T. J. Hammond, E. Frumker, R. W. Boyd, and P. B. Corkum, Phys. Rev. Lett. **113**, 153901 (2014).
14. R. Géneaux, A. Camper, T. Auguste, O. Gobert, J. Caillat, R. Taïeb, and T. Ruchon, Nat. Comm. **7**, 12583 (2016).
15. A. Denoeud, L. Chopineau, A. Leblanc, and F. Quéré, Phys. Rev. Lett. **118**, 033902 (2017).
16. X. Zhang, B. Shen, Y. Shi, X. Wang, L. Zhang, W. Wang, J. Xu, L. Yi, and Z. Xu, Phys. Rev. Lett. **114**, 173901 (2015).
17. C. Hernández-García, A. Picón, J. San Román, and L. Plaja, Phys. Rev. Lett. **111**, 083602 (2013).
18. P. R. Ribič, B. Rösner, D. Gauthier, E. Allaria, F. Döring, L. Foglia, L. Giannessi, N. Mahne, M. Manfredda, C. Masciovecchio *et al.*, Phys. Rev. X **7**, 031036 (2017).
19. A. Y. Bekshaev and A. I. Karamoch, Opt. Comm. **281**, 1366 (2008).
20. A. D'Errico, R. D'Amelio, B. Piccirillo, F. Cardano, and L. Marrucci, Optica. **4**, 1350 (2017).
21. F. Kong, C. Zhang, F. Bouchard, Z. Li, G. G. Brown, D. H. Ko, T. Hammond, L. Arissian, R. W. Boyd, E. Karimi *et al.*, Nat. Comm. **8**, 14970 (2017).
22. J. Zhang, S.-J. Huang, F.-Q. Zhu, W. Shao, and M.-S. Chen, Appl. Opt. **56**, 3556 (2017).
23. D. Gauthier, P. R. Ribič, G. Adhikary, A. Camper, C. Chappuis, R. Cucini, L. DiMauro, G. Dovillaire, F. Frassetto, R. Géneaux *et al.*, Nat. Comm. **8**, 14971 (2017).
24. F. Sanson, A. Pandey, F. Harms, G. Dovillaire, E. Baynard, J. Demailly, O. Guilbaud, B. Lucas, O. Neveu, M. Pittman *et al.*, Opt. Lett. **43**, 2780 (2018).
25. W. H. Southwell, J. Opt. Soc. Am. **70**, 998 (1980).
26. G. Vallone, Opt. Lett. **42**, 1997 (2017).
27. R. Géneaux, C. Chappuis, T. Auguste, S. Beaulieu, T. T. Gorman, F. Lepetit, L. F. DiMauro, and T. Ruchon, Phys. Rev. A **95**, 051801 (2017).
28. P. Balcou, P. Salières, A. L'Huillier, and M. Lewenstein, Phys. Rev. A **55**, 3204 (1997).
29. L. Rego, J. San Román, A. Picón, L. Plaja, and C. Hernández-García, Phys. Rev. Lett. **117**, 163202 (2016).

FULL REFERENCES

1. L. Huang, X. Song, B. Reineke, T. Li, X. Li, J. Liu, S. Zhang, Y. Wang, and T. Zentgraf, "Volumetric generation of optical vortices with metasurfaces," Acs Photonics **4**, 338–346 (2017).
2. L. Allen, M. W. Beijersbergen, R. Spreeuw, and J. Woerdman, "Orbital angular momentum of light and the transformation of laguerre-gaussian laser modes," Phys. Rev. A **45**, 8185 (1992).
3. R. Uren, S. Beecher, C. R. Smith, and W. A. Clarkson, "Method for generating high purity laguerre-gaussian vortex modes," IEEE J. Quantum Electron. (2019).
4. A. Rubano, F. Cardano, B. Piccirillo, and L. Marrucci, "Q-plate technology: a progress review," J. Opt. Soc. Am. B **36**, D70–D87 (2019).
5. T. W. Clark, R. F. Offer, S. Franke-Arnold, A. S. Arnold, and N. Radwell, "Comparison of beam generation techniques using a phase only spatial light modulator," Opt. Express **24**, 6249–6264 (2016).
6. T. Ando, Y. Ohtake, N. Matsumoto, T. Inoue, and N. Fukuchi, "Mode purities of laguerre–gaussian beams generated via complex-amplitude modulation using phase-only spatial light modulators," Opt. Lett. **34**, 34–36 (2009).
7. Y.-X. Ren, R.-D. Lu, and L. Gong, "Tailoring light with a digital micromirror device," Ann. Phys. **527**, 447–470 (2015).
8. M. Beijersbergen, "Helical-wavefront laser beams producted with a spiral phaseplate," Opt. Comm. **112**, 321–327 (1994).
9. K. Sueda, G. Miyaji, N. Miyanaga, and M. Nakatsuka, "Laguerre-gaussian beam generated with a multilevel spiral phase plate for high intensity laser pulses." Opt. Express **12**, 3548–53 (2004).
10. A. Longman and R. Fedosejevs, "Mode conversion efficiency to laguerre-gaussian oam modes using spiral phase optics," Opt. Express **25**, 17382–17392 (2017).
11. G. Machavariani, N. Davidson, E. Hasman, S. Blit, A. Ishaaya, and A. Friesem, "Efficient conversion of a gaussian beam to a high purity helical beam," Opt. Comm. **209**, 265–271 (2002).
12. Y. Shen, X. Wang, Z. Xie, and X. Yuan, "Optical vortices 30 years on: Oam manipulation from topological charge to multiple singularities," Light. Sci. & Appl. **8**, 90 (2019).
13. G. Gariepy, J. Leach, K. T. Kim, T. J. Hammond, E. Frumker, R. W. Boyd, and P. B. Corkum, "Creating high-harmonic beams with controlled orbital angular momentum," Phys. Rev. Lett. **113**, 153901 (2014).
14. R. Géneaux, A. Camper, T. Auguste, O. Gobert, J. Caillat, R. Taïeb, and T. Ruchon, "Synthesis and characterization of attosecond light vortices in the extreme ultraviolet," Nat. Comm. **7**, 12583 (2016).
15. A. Denoeud, L. Chopineau, A. Leblanc, and F. Quéré, "Interaction of ultraintense laser vortices with plasma mirrors," Phys. Rev. Lett. **118**, 033902 (2017).
16. X. Zhang, B. Shen, Y. Shi, X. Wang, L. Zhang, W. Wang, J. Xu, L. Yi, and Z. Xu, "Generation of intense high-order vortex harmonics," Phys. Rev. Lett. **114**, 173901 (2015).
17. C. Hernández-García, A. Picón, J. San Román, and L. Plaja, "Attosecond extreme ultraviolet vortices from high-order harmonic generation," Phys. Rev. Lett. **111**, 083602 (2013).
18. P. R. Ribič, B. Rösner, D. Gauthier, E. Allaria, F. Döring, L. Foglia, L. Giannessi, N. Mahne, M. Manfredda, C. Masciovecchio *et al.*, "Extreme-ultraviolet vortices from a free-electron laser," Phys. Rev. X **7**, 031036 (2017).
19. A. Y. Bekshaev and A. I. Karamoch, "Spatial characteristics of vortex light beams produced by diffraction gratings with embedded phase singularity," Opt. Comm. **281**, 1366 (2008).
20. A. D'Errico, R. D'Amelio, B. Piccirillo, F. Cardano, and L. Marrucci, "Measuring the complex orbital angular momentum spectrum and spatial mode decomposition of structured light beams," Optica. **4**, 1350–1357 (2017).
21. F. Kong, C. Zhang, F. Bouchard, Z. Li, G. G. Brown, D. H. Ko, T. Hammond, L. Arissian, R. W. Boyd, E. Karimi *et al.*, "Controlling the orbital angular momentum of high harmonic vortices," Nat. Comm. **8**, 14970 (2017).
22. J. Zhang, S.-J. Huang, F.-Q. Zhu, W. Shao, and M.-S. Chen, "Dimensional properties of laguerre–gaussian vortex beams," Appl. Opt. **56**, 3556–3561 (2017).
23. D. Gauthier, P. R. Ribič, G. Adhikary, A. Camper, C. Chappuis, R. Cucini, L. DiMauro, G. Dovillaire, F. Frassetto, R. Géneaux *et al.*, "Tunable orbital angular momentum in high-harmonic generation," Nat. Comm. **8**, 14971 (2017).
24. F. Sanson, A. Pandey, F. Harms, G. Dovillaire, E. Baynard, J. Demailly, O. Guilbaud, B. Lucas, O. Neveu, M. Pittman *et al.*, "Hartmann wavefront sensor characterization of a high charge vortex beam in the extreme ultraviolet spectral range," Opt. Lett. **43**, 2780–2783 (2018).
25. W. H. Southwell, "Wave-front estimation from wave-front slope measurements," J. Opt. Soc. Am. **70**, 998–1006 (1980).
26. G. Vallone, "Role of beam waist in laguerre–gauss expansion of vortex beams," Opt. Lett. **42**, 1997 (2017).
27. R. Géneaux, C. Chappuis, T. Auguste, S. Beaulieu, T. T. Gorman, F. Lepetit, L. F. DiMauro, and T. Ruchon, "Radial index of laguerre-gaussian modes in high-order-harmonic generation," Phys. Rev. A **95**, 051801 (2017).
28. P. Balcou, P. Salières, A. L'Huillier, and M. Lewenstein, "Generalized phase-matching conditions for high harmonics: The role of field-gradient forces," Phys. Rev. A **55**, 3204–3210 (1997).
29. L. Rego, J. San Román, A. Picón, L. Plaja, and C. Hernández-García, "Nonperturbative twist in the generation of extreme-ultraviolet vortex beams," Phys. Rev. Lett. **117**, 163202 (2016).